Earth and Planetary Science Letters 496 (2018) 108–119

Contents lists available at ScienceDirect

Earth and Planetary Science Letters

www.elsevier.com/locate/epsl

Reconstructing mantle carbon and noble gas contents from degassed mid-ocean ridge basalts

Jonathan M. Tucker [a,b,*], Sujoy Mukhopadhyay [c], Helge M. Gonnermann [d]

[a] Department of Earth and Planetary Sciences, Harvard University, 20 Oxford St., Cambridge, MA 02138, USA
[b] Department of Terrestrial Magnetism, Carnegie Institution for Science, 5241 Broad Branch Road NW, Washington, DC 20015, USA
[c] Department of Earth and Planetary Sciences, University of California Davis, One Shields Avenue, Davis, CA 95616, USA
[d] Department of Earth Science, Rice University, 6100 Main Street, Houston, TX 77005, USA

ARTICLE INFO

Article history:
Received 31 October 2017
Received in revised form 14 May 2018
Accepted 15 May 2018
Available online xxxx
Editor: T.A. Mather

Keywords:
degassing
mid-ocean ridges
noble gases
carbon
disequilibrium
volatiles

ABSTRACT

The fluxes of volatile elements from the mantle have long been used to understand mantle structure and evolution, and are critical controls on Earth's climate stability. Because of the ubiquity of magmatic degassing, inferring pre-degassing volatile concentrations from measured basalts requires the application of a degassing model. Such models, including the commonly-applied equilibrium Rayleigh distillation, typically assume equilibrium or solubility-based partitioning between melt and vapor. Here, we demonstrate that ratios of radiogenic isotopes of He, Ne, Ar and, especially, Xe measured in global mid-ocean ridge basalts (MORBs) are inconsistent with equilibrium degassing models, even when not considering He. We conclude that kinetic disequilibrium is a crucial process affecting volatile abundances during degassing. We present a simple disequilibrium Rayleigh distillation model to reconstruct pre-degassing MORB noble gas and carbon concentrations, which predicts that He and Ne achieve nearly equilibrium partitioning between melt and vesicles, but the slower-diffusing heavier noble gases are strongly affected by disequilibrium, resulting in non-equilibrium fractionation of noble gas elemental ratios, and other volatile element ratios like CO_2/He.

We apply our model to a large set of MORB data, and find average pre-degassing ^{3}He, ^{22}Ne, and ^{36}Ar concentrations of $4.4 \pm 0.9 \times 10^{-10}$, $6.6 \pm 1.4 \times 10^{-11}$, and $6.8 \pm 4.5 \times 10^{-10}$ ccSTP/g (2σ), with variations of approximately 2 orders of magnitude, similar to other highly incompatible elements. Pre-degassing noble gas concentrations imply a mid-ocean ridge ^{3}He flux of 800 ± 170 mol/yr and upper mantle ^{3}He/^{22}Ne and ^{3}He/^{36}Ar ratios of 6.6 ± 2.0 and 0.64 ± 0.44, but substantial variability in these ratios between samples. Applying our model to CO_2, we calculate an average mantle CO_2/^{3}He molar ratio of $1.67 \pm 0.21 \times 10^9$, which, when combined with our estimate of ^{3}He flux, implies an upper mantle CO_2 flux of $5.9 \pm 1.0 \times 10^{13}$ g/yr and a CO_2 concentration of approximately 110 ppm.

Our estimate of the mantle ^{3}He flux is the first determined independently of oceanographic ^{3}He measurements, and consequently represents a time-integrated flux substantially longer than ~1000 years. And although at the high end of the range of previous estimates, our estimate does not resolve the long-standing heat-helium paradox. Additionally, our requirement for heterogeneous pre-degassing ^{3}He/^{22}Ne and ^{3}He/^{36}Ar ratios between samples is contrary to conclusions of previous applications of disequilibrium degassing models, which advocated uniform ratios. Furthermore, we find that CO_2/Ba ratios are highly variable in MORB samples, but still consistent with an average mantle mass ratio of ~100. However, estimating pre-degassing CO_2 concentrations and the mantle CO_2 flux depend strongly on the poorly-constrained carbon diffusivity. Consequently, our demonstration of the prevalence of disequilibrium during mid-ocean ridge degassing, and the potential for disequilibrium in other volcanic settings, highlights the need for better characterization of the physical parameters associated with volcanic degassing.

1. Introduction

The abundances of volatile elements such as carbon, nitrogen, hydrogen, and noble gases place important constraints on the

* Corresponding author at: Department of Terrestrial Magnetism, Carnegie Institution for Science, 5241 Broad Branch Road NW, Washington, DC 20015, USA.
E-mail addresses: jtucker@carnegiescience.edu (J.M. Tucker), sujoy@ucdavis.edu (S. Mukhopadhyay), helge@rice.edu (H.M. Gonnermann).

https://doi.org/10.1016/j.epsl.2018.05.024
0012-821X/

provenance and timing of delivery of Earth's volatiles (Bergin et al., 2015; Marty, 2012; Morbidelli et al., 2000; Wänke, 1981). The flux of these volatiles between the mantle and surface affects climate stability and planetary habitability (Sleep and Zahnle, 2001; Walker et al., 1981). The mantle flux of He has long been used as a critical constraint on geodynamic modeling and the mantle structure (Gonnermann and Mukhopadhyay, 2009; Kellogg and Wasserburg, 1990; O'Nions and Oxburgh, 1983; Porcelli and Wasserburg, 1995; Tackley, 2015), and a means to establish fluxes and concentrations of other noble gases and elements such as C, N, S (Kagoshima et al., 2015; Marty, 1995, 2012; Marty and Dauphas, 2003; Marty and Tolstikhin, 1998; Trieloff and Kunz, 2005). The potential variability of nonradiogenic mantle noble gas elemental ratios is of interest to mantle dynamics, as uniform ratios are a requirement of "steady-state" mantle models (e.g., Porcelli and Ballentine, 2002), whereas heterogeneity may reflect a mantle incompletely mixed since Earth's accretion and/or different amounts of recycled atmospheric noble gases in mantle reservoirs (Caracausi et al., 2016; Kendrick et al., 2011, 2013; Mukhopadhyay, 2012; Mundl et al., 2017; Parai and Mukhopadhyay, 2015; Tucker and Mukhopadhyay, 2014).

While the budgets of volatiles in surface reservoirs (atmosphere, oceans, and crust) are relatively well quantified, concentrations in the mantle, and fluxes between the mantle and surface remain highly uncertain. Given the large size of the mantle, uncertainties in the mantle volatile concentrations render volatiles the least constrained aspect of the bulk silicate Earth composition.

Mid-ocean ridge basalts (MORBs) can serve as windows into the upper mantle composition. However, mantle volatile concentrations and fluxes are difficult to ascertain from measurements of oceanic basalts because many volatile species degas extensively prior to or during eruption. Consequently, MORB samples interpreted to have retained their pre-eruptive volatiles in vesicles, such as "popping rocks", are extremely rare (Hekinian et al., 2000; Javoy and Pineau, 1991). Similarly rare are MORBs that have not nucleated vesicles (Le Voyer et al., 2017; Michael and Graham, 2015; Saal et al., 2002; Shimizu et al., 2016), and the undegassed nature of these samples has been questioned (Matthews et al., 2017).

Noble gases are ideal tracers of magmatic degassing processes because of their inert nature and the systematic variation of physical properties such as solubility and diffusivity with mass. More importantly, the radiogenic noble gases $^{4}He^{*}$, $^{21}Ne^{*}$, $^{40}Ar^{*}$, and $^{136}Xe^{*}_{U}$ are produced from the radioactive decay of U, Th, and K at known rates ("*" denotes the radiogenic abundance, i.e. excluding atoms not produced by radioactive decay, and the subscript "U" denotes $^{136}Xe^{*}$ produced by spontaneous ^{238}U fission; Section 2; Supplementary Information §S1). Consequently, mantle ratios of radiogenic noble gases—referred to as mantle "production ratios"—are fixed, and deviations from these production ratios measured in MORBs can be attributed to elemental fractionation during degassing. In contrast, elemental ratios involving species like CO_2, N_2, or nonradiogenic noble gases can be affected by both degassing and heterogeneity in pre-degassing compositions.

Indeed, $^{4}He^{*}/^{40}Ar^{*}$ ratios measured in MORBs often differ substantially from the mantle production ratio, interpreted to result from solubility-controlled He/Ar fractionation experienced during degassing (Jambon et al., 1985). Furthermore, within the context of a solubility-based fractional degassing model, the extent of $^{4}He^{*}/^{40}Ar^{*}$ fractionation from the mantle production ratio is used to quantify the extent of degassing and predict pre-degassing concentrations of other volatiles, including CO_2 (e.g. Burnard, 2001; Burnard et al., 2014; Colin et al., 2013; Marty and Tolstikhin, 1998; Marty and Zimmermann, 1999; Section 5.3).

Considering multiple radiogenic noble gas ratios can provide stringent constraints on the nature of the degassing, as all noble gases are affected by the same processes. For example, a particular extent of equilibrium $^{4}He^{*}/^{40}Ar^{*}$ fractionation will be accompanied by a predictable extent of $^{4}He^{*}/^{21}Ne^{*}$ and $^{4}He^{*}/^{136}Xe^{*}_{U}$ fractionation. Here, we will show that this prediction is not met in the vast majority of MORBs, demonstrating that MORB degassing cannot be described by any solubility-based degassing model, including the widely-used equilibrium Rayleigh distillation model. We will argue that kinetic fractionation plays a critical role in controlling volatile abundances in MORBs and present a parameterized model for degassing by disequilibrium Rayleigh distillation. While our model is not meant to capture all physical processes associated with magmatism such as storage, transport, and eruption, it demonstrates the manner in which disequilibrium degassing can affect volatiles. We will use it to reconstruct pre-degassing noble gas and CO_2 concentrations in MORB magmas and the fluxes of these elements from the MORB mantle.

2. Equilibrium degassing models

We begin our discussion of mid-ocean ridge degassing by describing the most commonly applied equilibrium degassing models, and then testing them with a compilation of global MORB data.

2.1. Model description

The concentrations of volatiles in MORBs are controlled by diffusion of dissolved volatiles from the melt into CO_2-rich bubbles (Gerlach, 1989; Jambon et al., 1985; Sarda and Graham, 1990). Because noble gases are highly undersaturated in magmas, they do not nucleate bubbles, but rather partition into existing CO_2 bubbles. During closed-system degassing, bubbles remain with the melt from which they were derived. Given sufficient time for equilibration, a noble gas i partitions between melt and bubbles according to its solubility, quantified by Henry's constant k_i, the ratio of dissolved concentration in the melt C_i to partial pressure in the vapor P_i: $k_i = C_i/P_i$. Noble gas solubilities decrease with size (Jambon et al., 1986; Lux, 1987); consequently, during equilibrium closed-system degassing, He/Ne, He/Ar, and He/Xe ratios increase in residual melt, where the maximum amount of fractionation is the ratio of solubilities (Jambon et al., 1986).

If buoyant bubbles rise independently of melts, for example if melts stall or ascend slowly, open-system degassing may occur and noble gas fractionations in residual melts larger than solubility ratios is possible. The possibility of open-system degassing via multiple stages of bubble formation and loss presents a challenge to uniquely constrain the degassing history of a sample. To simplify the problem, a particular degassing model is often assumed wherein exsolved volatiles are continuously lost from the magma. This process, described mathematically by Rayleigh distillation, has been commonly used to model the evolution of volatile element ratios and C isotopes during MORB degassing (Burnard, 1999, 2001; Burnard et al., 2002, 2004, 2014; Cartigny et al., 2001, 2008; Colin et al., 2013; Javoy et al., 1982; Marty, 1995; Marty and Tolstikhin, 1998; Marty and Zimmermann, 1999; Parai et al., 2012; Pineau and Javoy, 1983; Pineau et al., 1976; Sarda and Graham, 1990).

Rayleigh distillation can be expressed in closed-form as an equation for the ratio of two volatile species during degassing

$$C_i/C_j = C_{i,0}/C_{j,0} \times f_i^{(1-\alpha_{ij})}. \quad (1)$$

Here $f_i = C_i/C_{i,0}$ is the concentration ratio of a dissolved volatile i in a melt to its pre-degassing concentration, and the fractionation factor $\alpha_{ij} = k_i/k_j$ is the ratio of solubilities. A full derivation of the equations describing the evolution of magmatic compositions during Rayleigh distillation is provided in the Supplementary Information (§S2).

In the case of two different elemental ratios, Equation (1) can be solved for f_i to give (e.g. Burnard, 2001; Marty, 1995; see Eq. (S16))

$$(C_k/C_l)_0 = C_k/C_l \times \left[(C_i/C_j)/(C_i/C_j)_0\right]^{(\alpha_{il}-\alpha_{ik})/(1-\alpha_{ij})}. \quad (2)$$

If i and j are ^{4}He* and ^{40}Ar*, then the initial ratio $(C_i/C_j)_0$ is the mantle production ratio. Consequently, pre-degassing ratios of any two elements $(C_k/C_l)_0$, such as $CO_2/^3$He, can be determined solely from measured $CO_2/^3$He and ^{4}He*/^{40}Ar* ratios. This methodology is the basis for many estimates of pre-degassing $CO_2/^3$He ratios in MORBs, and consequently the upper mantle CO_2 concentration and flux (Burnard et al., 2014; Cartigny et al., 2001; Marty and Tolstikhin, 1998; Marty and Zimmermann, 1999).

The mantle production ratios, $(C_i/C_j)_0$, are functions of the relative concentrations of parent isotopes (^{40}K, ^{232}Th, ^{235}U, ^{238}U), their decay constants, nuclear production yields, and mantle residence times. $(^4\text{He}^*/^{40}\text{Ar}^*)_0$ could range from approximately 1.1 to 4.4 due to variability in mantle K/U ratios and residence times (Supplementary Information §S1). Here, we assume $(^4\text{He}^*/^{40}\text{Ar}^*)_0 = 2.5$ but note that using different values has little effect on our results (Supplementary Information §S1). In contrast, $(^4\text{He}^*/^{21}\text{Ne}^*)_0$ and $(^4\text{He}^*/^{136}\text{Xe}^*_U)_0$ are nearly independent of composition and residence time (e.g., Šrámek et al., 2017). We use $(^4\text{He}^*/^{136}\text{Xe}^*_U)_0 = 3.5\times10^8$ (Graham, 2002; Ragettli et al., 1994) and $(^4\text{He}^*/^{21}\text{Ne}^*)_0 = 2.2 \times 10^7$ (Yatsevich and Honda, 1997), which falls within the uncertainty of the most recent determination of $2.38 \pm 0.26 \times 10^7$ (Šrámek et al., 2017).

To determine radiogenic noble gas concentrations in samples, corrections for nonradiogenic (i.e. primordial) and shallow-level atmospheric contaminant and/or recycled gases are required. For ^{4}He*, there is only a minimal contribution from nonradiogenic ^{4}He; for ^{21}Ne*, the nonradiogenic and atmospheric contaminant contributions can be significant; and for ^{40}Ar*, the contributions from atmospheric contaminant and recycled air can be significant. The equations used for calculating ^{4}He*, ^{21}Ne*, and ^{40}Ar* from measured noble gas compositions are discussed by Graham (2002) and given in the Supplementary Information (§S1).

Constraining degassing processes using ^{136}Xe*$_U$ has been not been previously accomplished due to the analytical difficulties involved (e.g. Burnard, 2001). Calculation of ^{136}Xe*$_U$ requires first computing ^{136}Xe* by subtracting primordial, recycled atmospheric, and atmospheric contaminant ^{136}Xe, and then deconvolving ^{136}Xe* contributions from U-fission and Pu-fission. These calculations are possible only for a handful of MORBs (Parai and Mukhopadhyay, 2015). For applicability to additional samples, we use an approximate calculation of ^{136}Xe* (Graham, 2002), with a factor discriminating U- from Pu-derived ^{136}Xe*:

$$^{136}\text{Xe}^*_U = {}^{130}\text{Xe}_{meas}\left(\left(^{136}\text{Xe}/^{130}\text{Xe}\right)_{meas} - \left(^{136}\text{Xe}/^{130}\text{Xe}\right)_{air}\right) \times {}^{136}\text{Xe}^*_U/{}^{136}\text{Xe}^*_{U+Pu} \quad (3)$$

This equation assumes all measured ^{130}Xe is atmospheric, either contaminant or recycled. On average, ~90% of the non-contaminant (i.e. mantle-derived) ^{130}Xe in oceanic basalts derives from recycled atmosphere, the remainder being primordial (Parai and Mukhopadhyay, 2015). Hence, assuming all measured ^{130}Xe is atmospheric (recycled plus contaminant) does not result in significant error in calculating ^{136}Xe*. We assume the uranogenic ^{136}Xe* (i.e., ^{136}Xe*$_U$/^{136}Xe*$_{U+Pu}$) = 0.7, the median MORB value (Parai and Mukhopadhyay, 2015).

2.2. Tests of equilibrium degassing models

While many studies have used the ^{4}He*/^{40}Ar* ratio to correct measured elemental ratios for degassing using the equilibrium Rayleigh distillation model (Equation (2)), the myriad radiogenic noble gas ratios, such as those including ^{21}Ne* and ^{136}Xe*$_U$, offer stringent predictive tests of the model.

Considering the radiogenic noble gas ratios ^{4}He*/^{40}Ar* and ^{4}He*/^{21}Ne*, Equation (2) defines a line (e.g., Burnard, 2001)

$$\log\left(^4\text{He}^*/^{40}\text{Ar}^*\right) = \frac{1-\alpha_{He,Ar}}{1-\alpha_{He,Ne}}\left[\log\left(^4\text{He}^*/^{21}\text{Ne}^*\right) - \log\left(^4\text{He}^*/^{21}\text{Ne}^*\right)_0\right] + \log\left(^4\text{He}^*/^{40}\text{Ar}^*\right)_0. \quad (4)$$

This line passes through the pre-degassing melt composition (the mantle production ratios) and its slope depends only on the α values. The distance along the line is related to the fractional degree of degassing, f_{He}. The instantaneous ratios of exsolved noble gases in bubbles follow a parallel path, offset by a factor of α (Supplementary Information, Equations (S16)–(S18)).

Fig. 1 demonstrates that the equilibrium Rayleigh distillation model cannot describe the vast majority of MORB data. Fig. 1 presents various ratios of ^{4}He*, ^{21}Ne*, ^{40}Ar*, and ^{136}Xe*$_U$ (calculated using Equations (3), (S1)–(S4)) from a compilation of published MORB data, the equilibrium Rayleigh distillation trajectory for dissolved radiogenic noble gases (Equation (4)), and the range in trajectories considering uncertainties in noble gas solubility ratios. The vast majority of data points in Fig. 1 plot away from the path described by equilibrium Rayleigh distillation; especially so for ratios involving Xe (e.g. Fig. 1b).

Other forms of equilibrium degassing besides Rayleigh distillation have been advocated, but also cannot explain the data in Fig. 1. Closed-system degassing (Chavrit et al., 2014) transfers gases from melt to vesicles, and therefore would not change bulk elemental ratios (i.e., those measured by fusion) from the mantle production ratios. Closed system degassing followed by a single stage of vesicle loss (Moreira and Sarda, 2000; Sarda and Moreira, 2002) increases residual He/Ne and He/Ar ratios from their initial values by at most factors of ~2 and ~10, the solubility ratios (Jambon et al., 1986; Lux, 1987). However, observed ratios have increased by up to ~10× and ~100× (Fig. 1), requiring open-system gas loss beyond a single stage. Likewise, closed-system degassing followed by equilibrium Rayleigh distillation (Cartigny et al., 2008), or step-wise (as opposed to continuous) open-system degassing do not intersect the majority of the data (Fig. S5). Finally, equilibrium degassing and mixing of undegassed magmas (Matthews et al., 2017) cannot reproduce the majority of natural compositions, as it cannot produce ^{40}Ar*/^{21}Ne* and ^{136}Xe*$_U$/^{21}Ne* ratios greater than the mantle production ratio (Fig. 1c). In fact, because equilibrium degassing decreases Ar/Ne and Xe/Ne ratios (Section 2.1), samples with ^{40}Ar*/^{21}Ne* and ^{136}Xe*$_U$/^{21}Ne* ratios greater than the mantle production ratios are extremely difficult to explain with any equilibrium model.

The He–Ne–Ar–Xe data might be explained by equilibrium degassing with solubilities different from experimentally-determined values (Burnard, 1999; Moreira and Sarda, 2000; Sarda and Moreira, 2002). However, some samples in Fig. 1 with approximately equal relative extents of He/Ne, He/Ar, and He/Xe fractionation would require solubility ratios of unity. There is currently no experimental evidence to support such extreme solubility ratios, or the degree of variability in solubility ratios required to explain the overall data scatter.

The deviation of noble gas ratios involving He from equilibrium degassing trajectories have been previously observed and interpreted to reflect anomalous behavior of He, such as diffusive fractionation of He from other noble gases during mantle melting or melt migration (Burnard, 2004; Matsuda and Marty, 1995), or exclusion from crystallizing minerals during oceanic crust formation

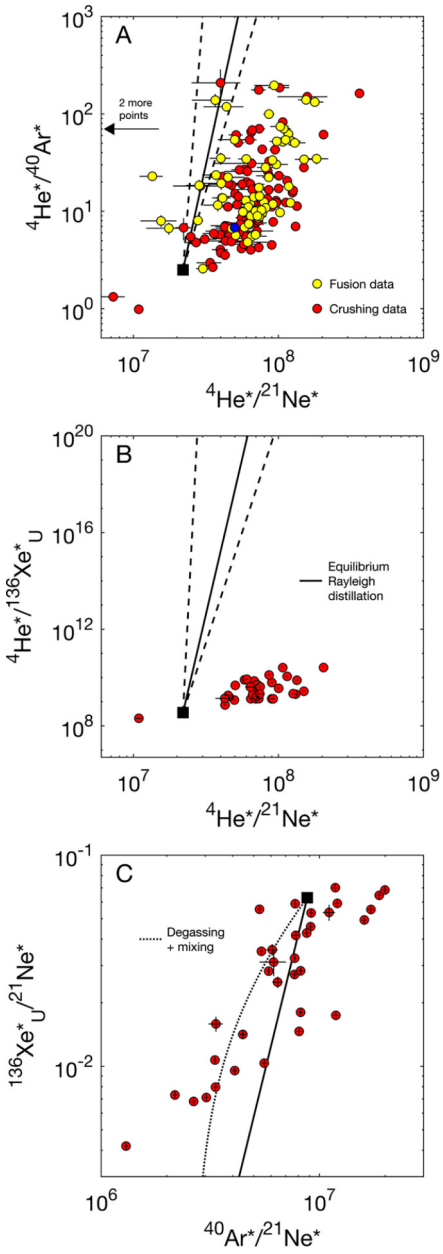

Fig. 1. (a) $^4He^*/^{40}Ar^*$ vs. $^4He^*/^{21}Ne^*$ in literature fusion (yellow, $n = 67$) and crushing (red, $n = 104$) data; (b) $^4He^*/^{136}Xe^*_U$ vs. $^4He^*/^{21}Ne^*$ ($n = 34$) and (c) $^{136}Xe^*_U/^{21}Ne^*$ vs. $^{40}Ar^*/^{21}Ne^*$ ($n = 34$). The blue point is AMK3376, referred to in Section 2.3. Crushing data are bulk compositions, i.e. the sum of individual crushing steps. Error bars (1σ) reflect propagated uncertainty from elemental concentrations. Also plotted are the compositional evolution of melt via equilibrium Rayleigh distillation using the solubilities of Jambon et al. (1986) (solid line) and Lux (1987) and Guillot and Sator (2012) (dashed lines, removed in (c) for clarity). Initial melt compositions (squares) are the mantle production ratios. The scatter implies that equilibrium Rayleigh distillation cannot explain the data using any fixed solubility ratios. Furthermore, much of the natural data plot far from the possible equilibrium paths, indicating that equilibrium Rayleigh distillation cannot explain the majority of the data with any reasonable solubility ratios. Panel (c) shows that non-equilibrium behavior does not result from anomalous behavior of He, and that mixing of partially degassed and undegassed melts (dotted line) does not reproduce the natural data. Data from Barry and Hilton (2016), Burnard et al. (2002, 2003, 2004), Colin et al. (2011), Füri et al. (2011), Hiyagon et al. (1992), Moreira and Allègre (2002), Moreira et al. (1995, 1996, 1998, 2011), Niedermann and Bach (1998), Niedermann et al. (1997), Parai et al. (2012), Pető (2014), Raquin and Moreira (2009), Sarda et al. (2000), Stroncik and Niedermann (2016), Stroncik et al. (2007), and Tucker et al. (2012); and listed in Table S1. Calculation of radiogenic abundances from raw data are described in Section 2.1 and the Supplementary Information (§S1). (For interpretation of the colors in the figure(s), the reader is referred to the web version of this article.)

(Honda and Patterson, 1999). However, Fig. 1c shows that deviations from equilibrium degassing are observed not just in ratios involving He but also in Ne–Ar–Xe spaces. Hence, a physical process beyond equilibrium degassing affects all of the noble gases. We argue that this process is disequilibrium degassing (Section 3), and conclude that equilibrium Rayleigh distillation, or any type of equilibrium model, cannot explain the vast majority of measured MORB He–Ne–Ar–Xe compositions.

2.3. Degassing paths from individual vesicles

Whereas the crushing and fusion data shown in Fig. 1 are bulk analysis techniques, further insights into degassing processes can be gleaned from compositions of individual vesicles within MORBs. Variations in vesicle ^4He–$^{40}Ar^*$–CO_2 compositions within some individual MORBs have been interpreted to result from equilibrium Rayleigh distillation (Burnard, 1999; Colin et al., 2013). This appears to contradict our conclusion that equilibrium Rayleigh distillation cannot explain MORB He–Ne–Ar–Xe compositions (Section 2.2, Fig. 1). Unlike in $^4He^*$–$^{21}Ne^*$–$^{40}Ar^*$–$^{136}Xe^*_U$ spaces, the initial composition in ^4He–$^{40}Ar^*$–CO_2 space is not fixed because mantle $^4He/CO_2$ or $^{40}Ar^*/CO_2$ ratios may be variable. Instead, to test the model, the solubility ratio k_{He}/k_{CO_2} required to match the vesicle data can be compared to experimental values. This empirical ratio ranges from ~1 to 5 with 1σ uncertainties close to 100% (Burnard, 1999; Colin et al., 2013), while the experimental ratio is ~2. Therefore, while individual vesicle data have been interpreted to be broadly consistent with an equilibrium Rayleigh distillation model, the variations and large uncertainties in empirical k_{He}/k_{CO_2} leave room for the possibility of non-equilibrium models.

Fig. 1 shows that tight constraints on degassing processes are afforded by the simultaneous analysis of three or more radiogenic noble gases. However, Ne analyses from single vesicles are extremely challenging. Ne analyses by crushing are available for a single sample also analyzed for ^4He–$^{40}Ar^*$–CO_2 in individual vesicles (AMK3376; Burnard, 2001), but this sample plots well away from the equilibrium Rayleigh distillation path (Fig. 1a, blue point), supporting our conclusion for a non-equilibrium process. Overall, we suggest that tight constraints on the degassing path afforded by $^4He^*/^{21}Ne^*$ makes acquisition of Ne data on single vesicles, or at the least from bulk crushing of the same sample, a high priority in refining models of magmatic degassing.

3. Kinetic fractionation during degassing

In the following sections, we present a parameterized disequilibrium degassing model that improves the fit to observed noble gas ratios in MORBs. The model allows us to reconstruct pre-degassing noble gas and CO_2 concentrations and explore the consequences of uncertainties in the physical parameters that control degassing.

3.1. Effects of kinetic fractionation

During equilibrium degassing, noble gases diffuse into bubbles until their dissolved concentrations correspond to their solubilities at the given partial pressure in the bubble. If there is insufficient time for all species to attain equilibrium partitioning, slower-diffusing species may not fully exsolve, resulting in non-equilibrium fractionations between faster and slower-diffusing species. Disequilibrium degassing has been argued to affect noble gas elemental ratios in OIBs (Gonnermann and Mukhopadhyay, 2007; Hanyu et al., 2005; Weston et al., 2015) and may also be important in MORBs (Aubaud et al., 2004; Burnard et al., 2003; Gonnermann and Mukhopadhyay, 2007; Paonita and Martelli, 2007; Pineau and Javoy, 1994), consistent with observed

CO_2 supersaturation in most MORBs (Dixon and Stolper, 1995; Stolper and Holloway, 1988).

Because larger noble gases are less soluble but diffuse at slower rates (Lux, 1987; Guillot and Sator, 2012), disequilibrium fractionates noble gases in the opposite sense of solubility. For example, the melt He/Ar ratio increases during equilibrium degassing, but disequilibrium inhibits Ar exsolution more than He, suppressing or even reversing this increase. Consequently, disequilibrium would affect He/Xe ratios the most and He/Ne the least. Disequilibrium can therefore explain why the MORB data tend to have lower $^4He^*/^{40}Ar^*$ and $^4He^*/^{136}Xe^*_U$ for a given $^4He^*/^{21}Ne^*$ than predicted by equilibrium models, and why some samples have $^{40}Ar^*/^{21}Ne^*$ ratios greater than the mantle production ratio (Fig. 1).

The potential for disequilibrium to lessen or reverse equilibrium fractionation represents a significant caveat to using the $^4He^*/^{40}Ar^*$ ratio to quantify extents of degassing. During disequilibrium degassing, the magmatic $^4He^*/^{40}Ar^*$ ratio could remain relatively constant even while significant volatile loss and fractionation of other elemental ratios occurs. A measured $^4He^*/^{40}Ar^*$ ratio close to the mantle production ratio could therefore be misinterpreted to represent a low extent of degassing (Aubaud et al., 2004; Paonita and Martelli, 2007; Weston et al., 2015).

3.2. A model for degassing by disequilibrium Rayleigh distillation

We present a simple model of disequilibrium degassing that can fit the MORB data with a minimum number of assumptions. We assume the simplest possible open-system degassing formulation whereby degassing proceeds by Rayleigh distillation, i.e. repeated closed-system degassing steps followed by bubble loss. But as volatile partitioning between melt and bubbles may be kinetically limited, α values are not strictly defined by solubilities. To quantify the extent of disequilibrium at each step, we employ the parameter θ, introduced by Gonnermann and Mukhopadhyay (2007):

$$\theta = \frac{8}{\pi^2}\sum_{j=0}^{\infty}\frac{1}{(2j+1)^2}e^{-D(2j+1)^2\pi^2(t/4a^2)}. \quad (5)$$

The quantity $(1-\theta)$ represents the fraction of a species that diffuses across a boundary (i.e. into a bubble) within time t (Supplementary Information, §2.2). θ is also a function of the diffusivity D of a volatile species (which itself may depend on parameters such as temperature and magmatic composition) as well as the characteristic diffusive length scale a, in an idealized sense, the half-distance between adjacent bubbles. For algebraic simplicity, we refer jointly to the time and length parameters as $\beta = t/a^2$.

In our model, a quantity $(1-\theta)$ for each volatile species determines its extent of disequilibrium by scaling its solubility, giving $C_i/P_i = k_i/(1-\theta_i)$ (Equation (S23)). C_i, P_i, and k_i are the dissolved concentration, vapor phase partial pressure, and equilibrium solubility of volatile species i. As θ approaches 0, from large β and/or D, this equation becomes Henry's law, and as θ approaches 1, due to small β and/or D, the volatile species is effectively not degassed and its dissolved concentration remains unchanged. Therefore, our model is simply disequilibrium Rayleigh distillation with "effective" solubilities $k' = k/(1-\theta)$ (Equation (S24)). Disequilibrium degassing paths are still calculated from Equation (4), although α values, and hence the degassing path slope, depend on solubilities, diffusivities, and β. As with equilibrium Rayleigh distillation, the distance traversed along the degassing path depends on the extent of degassing, quantified here by f_{He}.

β is a complicated function of the dynamics of vesiculation and eruption and may vary from sample to sample, but we assume β is constant for a given sample. We also assume that solubility ratios and diffusivities are constant, which is considered a reasonable approximation for MORBs (Weston et al., 2015; Yamamoto and Burnard, 2005). Therefore, the evolution of noble gas ratios during disequilibrium degassing can be modeled using two free parameters, β and f_{He}.

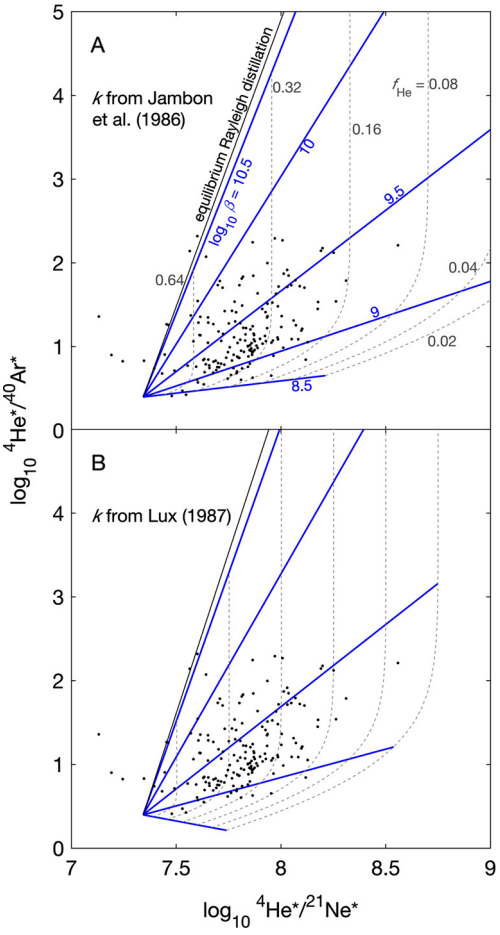

Fig. 2. Example disequilibrium Rayleigh distillation paths (blue) with variable β (blue text). At large values of β, the model approaches equilibrium Rayleigh distillation. Grey dashed lines are increments of constant f_{He}, the extent of He retention along a degassing path. The data are as in Fig. 1a, with error bars removed for clarity. The stronger kinetic retention of Ar compared to He and Ne explains why the samples and disequilibrium paths fall below and to the right of the equilibrium path. The diffusivities used are $D_{He} = 10^{-8.5}$, $D_{Ne} = 10^{-9.0}$, $D_{Ar} = 10^{-10.5}$ m^2/s; solubilities in (a) are from Jambon et al. (1986) and in (b) from Lux (1987). The two panels demonstrate that the disequilibrium Rayleigh distillation model can fit the data, although the required values of β and f_{He} depend on the values of solubility and diffusivity used.

Fig. 2 demonstrates that introducing disequilibrium adds a degree of freedom which allows our degassing model to reproduce nearly all MORB data. Fig. 2 shows degassing paths with different values of β plotted using our disequilibrium version of Equation (4). With decreasing β, the degassing paths diverge from equilibrium because He/Ar ratios are more strongly influenced by disequilibrium than He/Ne ratios. The majority of sample compositions in Fig. 2 can be reproduced by varying β within one order of magnitude and if up to 90% of initially dissolved He is lost from the magma.

Our new disequilibrium model is an idealized representation of a potentially protracted degassing process in nature. It differs from Gonnermann and Mukhopadhyay (2007) and Weston et al. (2015) in assuming continuous degassing rather than a discrete degassing steps, with the degassing extent f_{He} independent of CO_2 and of carbon diffusivity. Because the model can reproduce the majority of MORB data (Fig. 2), inclusion of additional degassing processes

Table 1
Summary of reconstructed volatile concentrations and associated model parameters.

	Mean	2σ	Median	2σ	1σ range		2σ range	
$\log_{10}\beta$	9.34	0.05	9.30	0.07	9.09	9.70	8.62	10.07
f_{He}	0.40	0.02	0.38	0.02	0.27	0.54	0.16	0.75
f_{Ne}	0.16	0.02	0.12	0.02	0.06	0.27	0.02	0.52
f_{Ar}	0.10	0.02	0.08	0.02	0.02	0.20	0.00	0.41
f_C	0.30	0.02	0.28	0.03	0.16	0.43	0.07	0.63
θ_{He}	3.0×10^{-3}	2.7×10^{-3}	1.3×10^{-7}	6.6×10^{-7}	1.2×10^{-17}	5.2×10^{-5}	4.4×10^{-40}	3.1×10^{-2}
θ_{Ne}	3.3×10^{-2}	1.2×10^{-2}	5.7×10^{-3}	4.8×10^{-3}	3.8×10^{-6}	3.8×10^{-2}	1.9×10^{-13}	2.9×10^{-1}
θ_{Ar}	0.68	0.02	0.72	0.02	0.55	0.78	0.32	0.87
θ_C	0.29	0.30	0.30	0.05	0.07	0.44	0.00	0.67
$^3He_0$	4.36×10^{-10}	8.94×10^{-11}	2.22×10^{-10}	4.42×10^{-11}	8.53×10^{-11}	8.49×10^{-10}	2.52×10^{-11}	2.35×10^{-9}
$^{22}Ne_0$	6.57×10^{-11}	1.39×10^{-11}	3.77×10^{-11}	6.51×10^{-12}	1.41×10^{-11}	1.03×10^{-10}	3.66×10^{-12}	3.60×10^{-10}
$^{36}Ar_0$	6.83×10^{-10}	4.49×10^{-10}	3.53×10^{-10}	1.31×10^{-10}	2.48×10^{-10}	1.23×10^{-9}	1.14×10^{-10}	3.96×10^{-9}
$CO_{2\,0}$	1640	306	1606	493	1227	2215	841	2277
$(^3He/^{22}Ne)_0$	6.84*	0.39	6.55	0.43	4.62	9.33	2.73	12.43
$(^3He/^{36}Ar)_0$	0.72*	0.11	0.62	0.16	0.50	0.91	0.48	1.27

Subscript $_0$ indicates pre-degassing value. ^{3}He, ^{22}Ne, and ^{36}Ar in ccSTP/g (1 mol/g = 2.24×10^4 ccSTp/g); CO_2 in ppm.
Uncertainties are 2 standard errors calculated from 10^6 bootstrap resamples.
1σ and 2σ ranges correspond to middle 68.3 and 95.4 percentiles.
*Bulk ratios ($\mu^3He/\mu^{22}Ne$ and $\mu^3He/\mu^{36}Ar$) of 6.6 ± 2.0 and 0.64 ± 0.44 (2σ) are better estimates of upper mantle ratios.

or stages is unnecessary, especially given the lack of required constraints.

4. Pre-degassing noble gas concentrations in MORBs

We use our degassing model to quantitatively reconstruct pre-degassing noble gas concentrations, with the caveat that these values are subject to uncertainty in the physical parameters used. We then explore the consequences of varying the physical parameters on our estimates.

4.1. Methodology

To calculate pre-degassing volatile concentrations for each sample, we solve for values of β and f_{He} by applying Equation (1) twice, once using the $^4He^*/^{21}Ne^*$ ratio and once using the $^4He^*/^{40}Ar^*$ ratio. The joint solution minimizes the misfit between measured and predicted values of the $^4He^*/^{21}Ne^*$ and $^4He^*/^{40}Ar^*$ ratios (Supplementary Information §S3). We use solubility constants from Jambon et al. (1986) and diffusivity constants $D_{He} = 10^{-8.5}$, $D_{Ne} = 10^{-9.0}$, and $D_{Ar} = 10^{-10.5}$ m^2/s, chosen from the middle of the ranges of experimental determinations (Lux, 1987; Nowak et al., 2004; Guillot and Sator, 2012; Fig. S3). The large scatter in the data (Fig. 2) requires that we fit β and f_{He} parameters for each individual sample, rather than a single degassing path slope (i.e. constant β) with variable f_{He}, contradicting previous degassing models which constrained MORB compositions to lie along a common degassing path (Moreira and Sarda, 2000). Including $^4He^*/^{136}Xe^*_U$ as additional constraint is currently premature because Xe is strongly affected by disequilibrium (Fig. 1b) and, therefore, strongly dependent on its poorly-known diffusivity and solubility (Supplementary Information §S4).

We calculate pre-degassing ^{3}He concentrations from the fitted values of f_{He} and measured ^{3}He concentrations (Table S1). The extent of retention of other volatile species, such as f_{Ne} or f_{Ar}, are calculated by $f_X = f_{He}^{\alpha_{He,X}}$ (Equations (1) and (S14)). To calculate pre-degassing ^{22}Ne and ^{36}Ar concentrations, measured ^{22}Ne and ^{36}Ar concentrations must first be corrected for atmospheric contamination, which requires mantle source $^{20}Ne/^{22}Ne$ and $^{40}Ar/^{36}Ar$ ratios. The former is often assumed to be ~12.5 in MORBs (e.g. Ballentine and Holland, 2008; Raquin et al., 2008), although this choice of value does not significantly affect our results (Fig. S1). We calculated the pre-degassing He and Ne concentrations for 159 of the 171 samples shown in Fig. 1a (Table S1). Samples plotting to the left of the equilibrium Rayleigh distillation path, such as the popping rock 2ΠD43, cannot be fit by our model and may necessitate additional processes such as He loss (Fig. S6). Reconstructing pre-degassing ^{36}Ar concentrations is possible only in 17 samples where mantle source $^{40}Ar/^{36}Ar$ ratios are known (Table S1).

Applying Equation (1) to model residual melt compositions is appropriate for fusion data, which measures total (vesicular + dissolved) volatiles, assuming any vesicles present formed in a last closed-system step subsequent to open-system bubble loss. In applying our methodology to samples measured by crushing, we assume that the noble gases are predominantly in vesicles. The pre-degassing concentrations determined would then represent a lower limit, because the dissolved noble gas concentrations would have to be added to reconstructed values. We note that this type of assumption is inherent in previous studies (e.g. Burnard, 1999; Marty and Tolstikhin, 1998; Marty and Zimmermann, 1999; Moreira and Sarda, 2000) and is justified in our dataset because the noble gas elemental ratios measured by crushing and by fusion are not systematically offset (Fig. 1a). Future work can improve upon the accuracy of our estimates by measuring the noble gas compositions in both vesicles and glass.

4.2. Results

All fitted β and f_{He} parameters and reconstructed pre-degassing compositions are given in Table S1, and a statistical summary presented in Table 1. MORB samples from all of the major ocean basin are included in our dataset, and the samples exhibit wide geochemical variability (Fig. S7). Thus, the statistics obtained from this set should be applicable to MORBs as a whole.

We estimate that, on average, samples lose 60% of their He, 84% of their Ne, and 90% of their Ar during degassing. θ_{He} and θ_{Ne} values close to 0 for most samples indicates that He and Ne were close to equilibrium. In contrast, the median θ_{Ar} value of 0.7 indicates that Ar experienced significant disequilibrium. Kr and Xe, which presumably have even lower diffusivities than Ar, would also experience strong disequilibrium.

Average pre-degassing ^{3}He, ^{22}Ne, and ^{36}Ar concentrations are 4.4 ± 0.9 × 10^{-10}, 6.6 ± 1.4 × 10^{-11}, and 6.8 ± 4.5 × 10^{-10} ccSTP/g, (uncertainties are 2 standard errors of the mean; Table 1; Fig. 3). Pre-degassing noble gas concentrations vary by approximately two orders of magnitude and follow log-normal distributions, similar to other highly incompatible elements, likely the result of variation in both the degree of melting and source composition (e.g. Arevalo and McDonough, 2010; Gale et al., 2013).

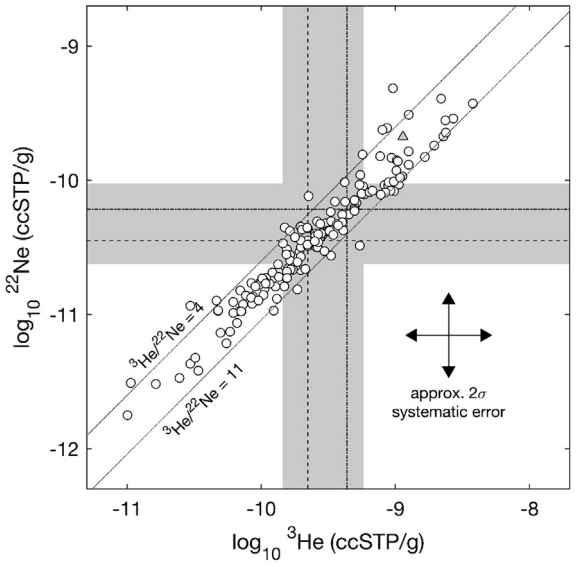

Fig. 3. Pre-degassing ^{3}He and ^{22}Ne contents of 159 MORB samples from Fig. 1 and Table S1, calculated using our disequilibrium degassing model, their mean values (dot-dashed lines) and median values (dashed lines). The grey triangle is the popping rock 2ΠD43 (Moreira et al., 1998), which has significantly more ^{3}He and ^{22}Ne than most MORBs, even after accounting for degassing. The grey bars show an independent estimate of the ^{3}He content of an average primary MORB magma of 0.98–3.9 $\times$ 10^{-10} and ^{22}Ne of 1.6–6.5 $\times$ 10^{-11} ccSTP/g (1 mol = 2.24 $\times$ 10^{4} ccSTP), derived from the oceanic ^{3}He flux ranging from 267 to 1070 mol/yr (Craig et al., 1975; Jean-Baptiste, 1992), an oceanic crust production rate of 21 km^{3}/yr (Crisp, 1984), ^{3}He/^{22}Ne of 6.1 (Tucker and Mukhopadhyay, 2014) and 32% crystallization (Michael and Graham, 2015). The arrows represent systematic uncertainty associated with solubility and diffusivity values; varying these values causes all points to shift en masse rather than randomly (Supplementary Information §S5).

4.3. Uncertainties in noble gas solubilities and diffusivities

Despite decades of experimental studies, solubilities and diffusivities of some volatiles are still uncertain to approximately an order of magnitude (Supplementary Information §S4). Rather than using a single set of values, as is done in most other studies, we assess the uncertainty associated with these values by varying them systematically in a grid search. This results in a conservative upper limit of a factor of 4 uncertainty (2σ) in pre-degassing ^{3}He and ^{22}Ne concentrations (Fig. 3; Supplementary Information §S5). We note that this uncertainty is systematic rather than random because varying solubility and diffusivity values affects all samples in a similar manner without changing the scatter between points. And importantly, because this uncertainty is due solely to the physical parameters, it is not an inherent limitation in our modeling approach. Therefore, better experimental constraints on solubility and diffusivity parameters will improve the accuracy of our reconstructions and improve our understanding of degassing in all volcanic environments.

5. Implications

5.1. Mantle noble gas fluxes

The mantle ^{3}He flux is used as a key constraint on geochemical and geodynamic modeling, and as a calibration for fluxes and concentrations of other volatiles. However, estimates of the mantle ^{3}He flux have been challenged on the basis that they are lower by at least a factor of 3–4 than that predicted based on the mantle radiogenic heat flux (van Keken et al., 2001; Ballentine et al., 2002); the so-called "heat-helium paradox" (O'Nions and Oxburgh, 1983). A long-term integrated ^{3}He flux significantly higher than the present-day flux is a possible resolution to this imbalance (van Keken et al., 2001; Ballentine et al., 2002), and could also obviate the need for a strongly chemically layered mantle (Ballentine et al., 2002).

We calculate the mantle ^{3}He flux to be 800 $\pm$ 170 mol/yr (2σ) based on our average pre-degassing ^{3}He concentration, 32% fractional crystallization (Michael and Graham, 2015), and an oceanic crust production rate of 21 km^{3}/yr (Crisp, 1984). We additionally calculate ^{22}Ne and ^{36}Ar fluxes of 120 $\pm$ 26, and 1260 $\pm$ 830 mol/yr. Previous estimates of the mantle ^{3}He flux, ranging from 267–1070 mol/yr (see Holzer et al., 2017) were obtained by combining oceanographic He measurements with models of ocean circulation. However, those fluxes integrate over just the past $\sim$1000 years, whereas our estimate, the first based on degassing-corrected ^{3}He measurements of MORBs, represents a much longer average flux of $\sim$10–100 ka. Although at the high end, our estimate is consistent with the range based on oceanographic measurements (e.g., grey bands in Fig. 3), suggesting that the modern flux is not a significant departure from the long-term average. We can therefore reject a high time-averaged He flux as a solution to the heat-helium paradox.

5.2. Heterogeneous mantle elemental ratios

The average and potential variability of nonradiogenic noble gas ratios in the mantle places important constraints on the origin of Earth's volatiles and mantle structure (Harper and Jacobsen, 1996; Honda and McDougall, 1998; Porcelli and Ballentine, 2002; Tucker and Mukhopadhyay, 2014). MORB mantle ^{3}He/^{22}Ne and ^{3}He/^{36}Ar ratios, calculated as the average ^{3}He concentration divided by the average ^{22}Ne or ^{36}Ar concentration, are 6.6 $\pm$ 2.0 and 0.64 $\pm$ 0.44. These values fall between independent estimates for the upper mantle ^{3}He/^{22}Ne and ^{3}He/^{36}Ar ratios of 6.1–7.3 and 0.4–0.8 (Graham, 2002; Holland and Ballentine, 2006; Honda and McDougall, 1998; Moreira et al., 1998; Tucker and Mukhopadhyay, 2014). These results lend confidence to our reconstructed concentrations, as the literature elemental ratios were determined through completely independent means.

Pre-degassing ^{3}He/^{22}Ne and ^{3}He/^{36}Ar ratios in individual samples are highly variable, ranging from 2.7 to 12.4 and 0.48 to 1.27 (2σ ranges; Table 1). Previous work has argued that variable elemental ratios measured in MORBs and OIBs could be explained through disequilibrium degassing of a uniform mantle noble gas ratio, supporting "steady-state" models (Paonita and Martelli, 2007; Weston et al., 2015). Pre-degassing ratios calculated using our model made no assumptions about nonradiogenic ratios like ^{3}He/^{22}Ne, and used both ^{4}He*/^{21}Ne* and ^{4}He*/^{40}Ar* as constraints, rather than just ^{4}He*/^{40}Ar*. Thus, the heterogeneity in pre-degassing ^{3}He/^{22}Ne and ^{3}He/^{36}Ar ratios we obtain contradicts the notion of uniform nonradiogenic mantle ratios. Our results concur with ^{3}He/^{22}Ne ratios calculated purely from ^{4}He/^{3}He and ^{21}Ne/^{22}Ne isotopic compositions (Honda and McDougall, 1998; Moreira and Sarda, 2000; Graham, 2002), which *require* different ^{3}He/^{22}Ne ratios for the mantle sources. Furthermore, some rare samples have ^{4}He*/^{21}Ne* and ^{4}He*/^{40}Ar* ratios similar to the mantle production ratios, suggesting they have not suffered elemental fractionation from degassing, yet still have distinct ^{3}He/^{22}Ne and ^{3}He/^{36}Ar ratios (Mukhopadhyay, 2012). We argue that because some degassing models can *fit* a subset of observed data with a uniform pre-degassing ^{3}He/^{22}Ne ratio, such an exercise does not necessarily imply that the ratio is indeed uniform.

5.3. The mantle carbon concentration and flux

The mantle carbon concentration and flux are critically important to biological and geological processes, but difficult to quantify due to the complications of magmatic degassing. These quantities

are often estimated from the average mantle ratio of carbon to another element such as $CO_2/^3He$ or CO_2/Ba. Our approach to reconstructing pre-degassing noble gas concentrations can also be applied to understanding the distribution of pre-degassing carbon concentrations in MORBs and the carbon flux from ridges.

5.3.1. Pre-degassing carbon concentrations and the mantle CO_2/Ba ratio

Recent work has shown that the CO_2/Ba mass ratio in undegassed MORBs is relatively constant around 100 (Hauri et al., 2017; Le Voyer et al., 2017; Michael and Graham, 2015; Rosenthal et al., 2015; Shimizu et al., 2016), making Ba a useful proxy for the mantle CO_2 flux. However, Matthews et al. (2017) questioned the undegassed nature of these samples, creating an impetus to independently constrain the potential variability of pre-degassing CO_2/Ba ratios.

To estimate pre-degassing CO_2/Ba ratios of individual samples, we calculate the extent of CO_2 retention, f_{CO_2}, during degassing by applying Equation S14, using the values of β and f_{He} fitted for each sample from $^4He^*$–$^{21}Ne^*$–$^{40}Ar^*$ data (Table S1). These calculations require values for k'_{CO2}, which depend on carbon solubility and diffusivity in basaltic magma. We use a solubility of 28 $\times$ 10^{-5} ccSTP/g/bar (Pan et al., 1991) and an empirically determined diffusivity of $10^{-9.7}$ m^2/s (Supplementary Information §S6), similar to values in Guillot and Sator (2011). We combine calculated f_{CO_2} with the total measured CO_2 concentration, comprising both vesicular and dissolved CO_2. The required noble gas and CO_2 data are available only for 10 samples (Table S1). Pre-degassing CO_2 concentrations in these samples range from 840 to 2280 ppm, with an average of 1640 ppm (Fig. 4a, Tables 1 and S1). This value is lower than 3850 ppm measured for the undegassed popping rock 2ΠD43 (Javoy and Pineau, 1991), but comparable to CO_2-rich melt inclusions in MORBs (Fig. 4b).

Fig. 4b shows our estimated pre-degassing CO_2 concentrations vs. Ba concentrations measured in the same samples along with literature data. CO_2/Ba ratios are quite variable in samples with average to high Ba concentrations, implying heterogeneity in mantle CO_2/Ba ratios. This heterogeneity is not a function of uncertainties in solubilities and diffusivities, including D_C, as those quantities affect pre-degassing estimates systematically rather than randomly.

The average CO_2/Ba mass ratios estimated for our samples is 103 $\pm$ 28, similar to previous estimates (Matthews et al., 2017; Michael and Graham, 2015; Rosenthal et al., 2015), obtained using a completely independent method. We recalculate the average for all MORB samples to be 98 $\pm$ 22 (2 standard errors). Therefore, while mantle CO_2/Ba ratios are more variable than previously recognized, an average value around 100 still appears applicable to samples spanning most of the MORB Ba concentration range. Therefore, our model supports the notion that undersaturated samples are truly undegassed rather than the consequence of mixing of partially degassed melts (Matthews et al., 2017; also see Fig. 1c). Consequently, while locally CO_2/Ba ratios are variable (Fig. 4), Ba is still an adequate global proxy for CO_2.

5.3.2. The mantle $CO_2/^3He$ ratio and CO_2 flux

The mantle $CO_2/^3He$ ratio, combined with the mantle ^3He flux, is the basis for many determinations of the mantle CO_2 flux and concentration. To determine pre-degassing ratios in MORBs, measured $CO_2/^3He$ ratios are often corrected for fractionation during degassing using an equilibrium Rayleigh distillation model based on the extent of $^4He^*/^{40}Ar^*$ fractionation from the mantle production ratio (Equation (2); Burnard et al., 2002; Colin et al., 2013; Marty and Jambon, 1987; Marty and Tolstikhin, 1998; Marty and Zimmermann, 1999; Parai et al., 2012). When applied to our 171 samples, equilibrium Rayleigh distillation predicts an average decrease in $CO_2/^3He$ ratios of just 18% during degassing. A similarly muted extent of fractionation has previously been suggested using

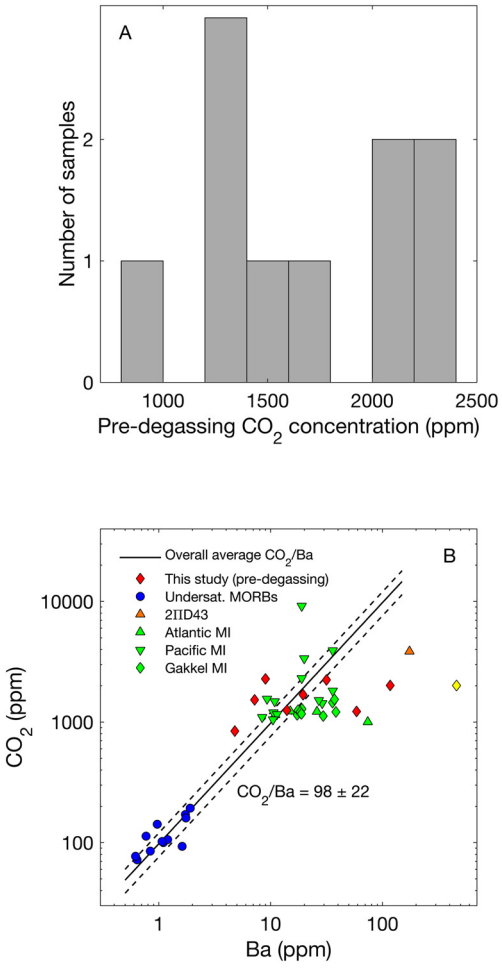

Fig. 4. (a) Pre-degassing CO_2 concentrations using our disequilibrium degassing model (Table S1). The values of 800–2300 ppm are similar to the most CO_2-rich melt inclusions in MORBs. (b) Pre-degassing CO_2 vs. Ba in our samples (red diamonds), along with undegassed MORB samples and CO_2-rich MORB melt inclusions. The yellow diamond is VAN7 89-02, which has an exceedingly high Ba concentration of 460 ppm. Blue circles are undersaturated MORBs excluding Gakkel Ridge samples (Michael and Graham, 2015); the orange triangle is the popping rock 2ΠD43 (Javoy and Pineau, 1991); green symbols are MORB melt inclusion data from Helo et al. (2011), Shaw et al. (2010), Wanless and Shaw (2012), and Wanless et al. (2014, 2015). The black solid and dashed lines are the average CO_2/Ba ratio from all samples and its uncertainty, which is similar to values of 105 $\pm$ 9 (Michael and Graham, 2015), 133 $\pm$ 44 (Rosenthal et al., 2015), and ~140 (Matthews et al., 2017).

the same methodology, resulting in the "canonical" average pre-degassing molar $CO_2/^3He$ of ~2 $\times$ 10^9 (Marty and Jambon, 1987; Marty and Tolstikhin, 1998; Marty and Zimmermann, 1999).

However, given the observation that equilibrium Rayleigh distillation fails to explain most MORB He–Ne–Ar–Xe compositions (Fig. 1), we assess the robustness of $CO_2/^3He$ reconstructions using our disequilibrium model. On average, CO_2/He ratios decrease during disequilibrium Rayleigh distillation by 26 $\pm$ 5% (2 standard errors), however, CO_2/He ratios in several samples actually *increase* during degassing (Fig. 5a, Table S1). For an average measured $CO_2/^3He$ ratio of 1.24 $\pm$ 0.23 $\times$ 10^9 (2 standard errors of the mean on 97 samples in Burnard et al., 2004; Marty and Tolstikhin, 1998; Marty and Zimmermann, 1999; Parai et al., 2012; Tucker et al., 2012), and a decrease of 26 $\pm$ 5% during degassing, we predict an average pre-degassing $CO_2/^3He$ ratio of 1.67 $\pm$ 0.21 $\times$ 10^9 (2σ), similar to the canonical value of 2 $\times$ 10^9.

The equilibrium and disequilibrium Rayleigh distillation models both predict relatively low average extents of CO_2/He fractionation during degassing, but for different reasons, so their apparent similarity is fortuitous. In the disequilibrium model, the ~2$\times$ lower

solubility of CO_2 compared to He is countered by its lower diffusivity, suppressing CO_2/He fractionation during degassing. Additionally, the extent of CO_2/He fractionation critically depends on the assumed D_C, which is poorly constrained. For example, Fig. 5b shows that the average pre-degassing MORB $CO_2/^3He$ ratio could be uncertain to a factor of 5 solely from different estimates of D_C, highlighting the critical need for a more accurate determination of carbon diffusivity in determining pre-degassing carbon concentrations. In the equilibrium model, He/Ar fractionations up to ~100× (Fig. 1a) result in only 10s of % of CO_2/He fractionation because $\alpha_{He,CO2}$ is much smaller than $\alpha_{He,Ar}$. Furthermore, an equilibrium model based on $^4He^*/^{21}Ne^*$ would predict CO_2/He fractionations of ~2–4×, rather than 10s of % predicted by $^4He^*/^{40}Ar^*$, due to similar solubilities of Ne and CO_2. And while both the disequilibrium and $^4He^*/^{40}Ar^*$-based equilibrium Rayleigh distillation models predict a low *average* extent of CO_2/He fractionation, predictions for individual samples do not necessarily correspond. Hence equilibrium Rayleigh distillation should not be used to predict pre-degassing $CO_2/^3He$ ratios.

We estimate an upper mantle CO_2 flux of $5.9 \pm 1.0 \times 10^{13}$ g/yr (2σ) based on our average pre-degassing MORB $CO_2/^3He$ ratio of $1.67 \pm 0.21 \times 10^9$ and ^3He flux of 800 ± 170 (Section 4.2). Assuming an average of 10% partial melting (e.g. Klein and Langmuir, 1987; Johnson et al., 1990), the CO_2 flux corresponds to a MORB mantle CO_2 concentration of 110 ppm. Similarly, using D_C from Guillot and Sator (2011), the CO_2 flux is 4.8×10^{13} g/yr and mantle CO_2 concentration is 80 ppm. However, our model results demonstrate (Fig. 5b) that obtaining tighter constraints on pre-degassing $CO_2/^3He$ ratios and the mantle CO_2 concentration and flux will require better characterization of the carbon diffusivity in basaltic melt.

6. Conclusions

Combining the use of $^{136}Xe^*_U$ with other noble gases in MORBs, we demonstrate that radiogenic noble gas ratios place stringent constraints on degassing processes, and do not support equilibrium degassing (Fig. 1). This observation invalidates equilibrium or solubility-based degassing models, including the often-used equilibrium Rayleigh distillation model. We propose that disequilibrium fractionation strongly affects noble gas elemental ratios during MORB degassing, and present a simple model of disequilibrium Rayleigh distillation capable of reproducing nearly all MORB noble gas data (Fig. 2) without requiring additional processes. This model predicts that He and Ne are little affected by disequilibrium, but CO_2, Ar, and presumably Kr and Xe, are moderately to strongly affected, owing to their lower magmatic diffusivities.

Applying our model to global MORB data, we demonstrate that pre-degassing ^3He, ^{22}Ne, and ^{36}Ar concentrations vary by approximately two orders of magnitude (Fig. 3), similar to other highly incompatible elements. Average pre-degassing magmas have $4.4 \pm 0.9 \times 10^{-10}$, $6.6 \pm 1.4 \times 10^{-11}$, and $6.8 \pm 4.5 \times 10^{-10}$ ccSTP/g ^3He, ^{22}Ne, and ^{36}Ar, respectively, implying a long-term mantle ^3He flux of 800 ± 170 mol/yr (2σ); the first such determination independent of oceanographic ^3He measurements. While on the high end of previous ^3He flux estimates, our estimate is still not high enough to resolve heat-helium paradox. We find upper mantle $^3He/^{22}Ne$ and $^3He/^{36}Ar$ ratios of 6.6 ± 2.0 and 0.64 ± 0.44, similar to independent estimates, although our results require approximately a factor of 3 variability in these ratios in the MORB mantle (Fig. 3). This heterogeneity contradicts the claim that variable noble gas elemental ratios observed in MORBs can be explained by disequilibrium degassing of a uniform mantle composition.

We find that predicting pre-degassing CO_2 concentrations, CO_2/Ba ratios, and the extent of $CO_2/^3He$ fractionation strongly depend on the poorly-constrained carbon diffusivity in basaltic melt.

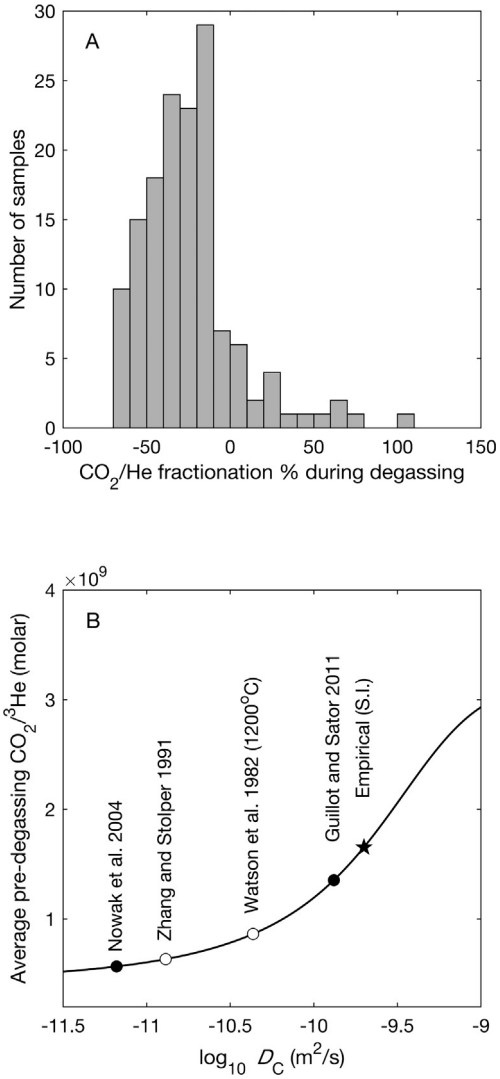

Fig. 5. (a) Extent of CO_2/He fractionation for 159 samples estimated using our disequilibrium degassing model. On average, CO_2/He ratios decrease by 26 ± 5% during degassing but some ratios actually increase. (b) Average MORB pre-degassing $CO_2/^3He$ ratio as a function of the carbon diffusivity assumed. For each value of D_C, we compute the extent of CO_2/He fractionation of our 159 samples using our disequilibrium degassing model (e.g. panel a). We then compute the average pre-degassing MORB $CO_2/^3He$ ratio from the average extent of CO_2/He fractionation in our samples and the average MORB $CO_2/^3He$ ratio of $1.24 \pm 0.23 \times 10^9$. The closed symbols indicate literature determinations of D_C (total; Guillot and Sator, 2011; Nowak et al., 2004) and our empirical determination (Supplementary Information §S6). The open symbols indicate literature determinations of carbonate diffusivity (Watson et al., 1982; Zhang and Stolper, 1991), which may underestimate D_C (total), as they do not include molecular CO_2. The figure demonstrates that while an average pre-degassing MORB value of 2×10^9 may not be inconsistent with our disequilibrium model, the precise value depends strongly on the poorly-constrained D_C.

Using an empirically-derived carbon diffusivity similar to some experimental determinations, we find significant heterogeneity in mantle CO_2/Ba ratios, although an average CO_2/Ba mass ratio of ~100 is still consistent with the data (Fig. 4). $CO_2/^3He$ ratios are little fractionated during disequilibrium degassing, resulting in an average pre-degassing $CO_2/^3He$ molar ratio of $1.67 \pm 0.21 \times 10^9$ (Fig. 5). From our estimates of average mantle $CO_2/^3He$ ratio and ^3He flux, we estimate an upper mantle CO_2 flux of $5.9 \pm 1.0 \times 10^{13}$ g/yr, and CO_2 concentration of 110 ppm.

The successful reproduction of a large global MORB noble gas data set with our simple degassing model provides strong support that disequilibrium is a ubiquitous feature of magmatic degassing. Consequently, the fundamental role of disequilibrium degassing in

global volatile cycles provides a strong impetus to better constrain solubilities and diffusivities of volatile elements in basaltic melts.

Acknowledgements

This paper is dedicated to the memory of Pete Burnard, whose pioneering work on magmatic degassing motivated our own study. We thank Erik Hauri and Kei Shimizu for thoughtful discussions; Simon Matthews, Bernard Marty, and an anonymous reviewer for constructive comments; and Tamsin Mather for editorial handling. The work was supported by NSF grant OCE 1464484 and a Deep Carbon Observatory postdoctoral fellowship to J.M.T.

Appendix A. Supplementary material

Supplementary material related to this article can be found online at https://doi.org/10.1016/j.epsl.2018.05.024.

References

Arevalo, R., McDonough, W.F., 2010. Chemical variations and regional diversity observed in MORB. Chem. Geol. 271, 70–85.
Aubaud, C., Pineau, F., Jambon, A., Javoy, M., 2004. Kinetic disequilibrium of C, He, Ar and carbon isotopes during degassing of mid-ocean ridge basalts. Earth Planet. Sci. Lett. 222, 391–406.
Ballentine, C.J., Holland, G., 2008. What CO_2 well gases tell us about the origin of noble gases in the mantle and their relationship to the atmosphere. Philos. Trans. R. Soc. Lond. A 336, 4183–4203.
Ballentine, C.J., van Keken, P.E., Porcelli, D., Hauri, E.H., 2002. Numerical models, geochemistry and the zero-paradox noble-gas mantle. Philos. Trans. R. Soc. Lond. A 360, 2611–2631.
Barry, P.H., Hilton, D.R., 2016. Release of subducted sedimentary nitrogen throughout Earth's mantle. Geochem. Perspect. Lett. 2, 148–159.
Bergin, E.A., Blake, G.A., Ciesla, F., Hirschmann, M.M., Li, J., 2015. Tracing the ingredients for a habitable earth from interstellar space through planet formation. Proc. Natl. Acad. Sci. USA 112, 8965–8970.
Burnard, P., 1999. The bubble-by-bubble volatile evolution of two mid-ocean ridge basalts. Earth Planet. Sci. Lett. 174, 199–211.
Burnard, P., 2001. Correction for volatile fractionation in ascending magmas: noble gas abundances in primary mantle melts. Geochim. Cosmochim. Acta 65, 2605–2614.
Burnard, P., 2004. Diffusive fractionation of noble gases and helium isotopes during mantle melting. Earth Planet. Sci. Lett. 220, 287–295.
Burnard, P.G., Graham, D.W., Farley, K.A., 2002. Mechanisms of magmatic gas loss along the Southeast Indian Ridge and the Amsterdam–St. Paul Plateau. Earth Planet. Sci. Lett. 203, 131–148.
Burnard, P.G., Graham, D.W., Farley, K.A., 2004. Fractionation of noble gases (He, Ar) during MORB melting: a case study on the Southeast Indian Ridge. Earth Planet. Sci. Lett. 227, 457–472.
Burnard, P., Harrison, D., Turner, G., Nesbitt, R., 2003. Degassing and contamination of noble gases in Mid-Atlantic Ridge basalts. Geochem. Geophys. Geosyst. 4, 1002.
Burnard, P., Reisberg, L., Colin, A., 2014. An observed link between lithophile compositions and degassing of volatiles (He, Ar, CO_2) in MORBs with implications for Re volatility and the mantle C/Nb ratio. Earth Planet. Sci. Lett. 395, 159–167.
Caracausi, A., Avice, G., Burnard, P.G., Füri, E., Marty, B., 2016. Chondritic xenon in the Earth's mantle. Nature 533, 82–85.
Cartigny, P., Jendrzejewski, N., Pineau, F., Petit, E., Javoy, M., 2001. Volatile (C, N, Ar) variability in MORB and the respective roles of mantle source heterogeneity and degassing: the case of the Southwest Indian Ridge. Earth Planet. Sci. Lett. 194, 241–257.
Cartigny, P., Pineau, F., Aubaud, C., Javoy, M., 2008. Towards a consistent mantle carbon flux estimate: Insights from volatile systematics (H_2O/Ce, δD, CO_2/Nb) in the North Atlantic mantle (14° N and 34° N). Earth Planet. Sci. Lett. 265, 672–685.
Chavrit, D., Humler, E., Grasset, O., 2014. Mapping CO_2 fluxes and mantle carbon content all along the mid-ocean ridge system. Earth Planet. Sci. Lett. 387, 229–239.
Colin, A., Burnard, P., Marty, B., 2013. Mechanisms of magma degassing at mid-oceanic ridges and the local volatile composition (^{4}He–^{40}Ar*–CO_2) of the mantle by laser ablation analysis of individual MORB vesicles. Earth Planet. Sci. Lett. 361, 183–194.
Colin, A., Burnard, P.G., Graham, D.W., Marrocchi, Y., 2011. Plume–ridge interaction along the Galapagos Spreading Center: discerning between gas loss and source effects using neon isotopic compositions and ^{4}He–^{40}Ar*–CO_2 relative abundances. Geochim. Cosmochim. Acta 75, 1145–1160.
Craig, H., Clarke, W.B., Beg, M.A., 1975. Excess ^{3}He in deep water on the East Pacific Rise. Earth Planet. Sci. Lett. 26, 125–132.
Crisp, J.A., 1984. Rates of magma emplacement and volcanic output. J. Volcanol. Geotherm. Res. 20, 177–211.
Dixon, J.E., Stolper, E.M., 1995. An experimental study of water and carbon dioxide solubilities in mid-ocean ridge basaltic liquids. Part II: applications to degassing. J. Petrol. 36, 1633–1646.
Füri, E., Hilton, D.R., Murton, B.J., Hémond, C., Dyment, J., Day, J., 2011. Helium isotope variations between Réunion Island and the Central Indian Ridge (17°–21° S): new evidence for ridge–hot spot interaction. J. Geophys. Res., Solid Earth 116, B02207.
Gale, A., Dalton, C.A., Langmuir, C.H., Su, Y., Schilling, J.G., 2013. The mean composition of ocean ridge basalts. Geochem. Geophys. Geosyst. 14, 489–518.
Gerlach, T.M., 1989. Degassing of carbon dioxide from basaltic magma at spreading centers: II. Mid-oceanic ridge basalts. J. Volcanol. Geotherm. Res. 39, 221–232.
Gonnermann, H.M., Mukhopadhyay, S., 2007. Non-equilibrium degassing and a primordial source for helium in ocean-island volcanism. Nature 449, 1037–1040.
Gonnermann, H.M., Mukhopadhyay, S., 2009. Preserving noble gases in a convecting mantle. Nature 459, 560–563.
Graham, D.W., 2002. Noble gas isotope geochemistry of mid-ocean ridge and ocean island basalts: characterization of mantle source reservoirs. Rev. Mineral. Geochem. 47, 247–317.
Guillot, B., Sator, N., 2011. Carbon dioxide in silicate melts: a molecular dynamics simulation study. Geochim. Cosmochim. Acta 75, 1829–1857.
Guillot, B., Sator, N., 2012. Noble gases in high-pressure silicate liquids: a computer simulation study. Geochim. Cosmochim. Acta 80, 51–69.
Hanyu, T., Clague, D.A., Kaneoka, I., Dunai, T.J., Davies, G.R., 2005. Noble gas systematics of submarine alkalic lavas near the Hawaiian hotspot. Chem. Geol. 214, 135–155.
Harper Jr., C.L., Jacobsen, S.B., 1996. Noble gases and Earth's accretion. Science 273, 1814–1818.
Hauri, E.H., Maclennan, J., McKenzie, D., Gronvold, K., Oskarsson, N., Shimizu, N., 2017. CO_2 content beneath northern Iceland and the variability of mantle carbon. Geology 46, 55–58.
Hekinian, R., Pineau, F., Shilobreeva, S., Bideau, D., Gracia, E., Javoy, M., 2000. Deep sea explosive activity on the Mid-Atlantic Ridge near 34°50′N: magma composition, vesicularity and volatile content. J. Volcanol. Geotherm. Res. 98, 49–77.
Helo, C., Longpré, M.A., Shimizu, N., Clague, D.A., Stix, J., 2011. Explosive eruptions at mid-ocean ridges driven by CO_2-rich magmas. Nat. Geosci. 4, 260–263.
Hiyagon, H., Ozima, M., Marty, B., Zashu, S., Sakai, H., 1992. Noble gases in submarine glasses from mid-oceanic ridges and Loihi seamount: constraints on the early history of the Earth. Geochim. Cosmochim. Acta 56, 1301–1316.
Holland, G., Ballentine, C.J., 2006. Seawater subduction controls the heavy noble gas composition of the mantle. Nature 441, 186–191.
Holzer, M., DeVries, T., Bianchi, D., Newton, R., Schlosser, P., Winckler, G., 2017. Objective estimates of mantle ^{3}He in the ocean and implications for constraining the deep ocean circulation. Earth Planet. Sci. Lett. 458, 305–314.
Honda, M., McDougall, I., 1998. Primordial helium and neon in the Earth—a speculation on early degassing. Geophys. Res. Lett. 25, 1951–1954.
Honda, M., Patterson, D.B., 1999. Systematic elemental fractionation of mantle-derived helium, neon, and argon in mid-oceanic ridge glasses. Geochim. Cosmochim. Acta 63, 2863–2874.
Jambon, A., Weber, H., Braun, O., 1986. Solubility of He, Ne, Ar, Kr and Xe in a basalt melt in the range 1250–1600°C. Geochemical implications. Geochim. Cosmochim. Acta 50, 401–408.
Jambon, A., Weber, H.W., Begemann, F., 1985. Helium and argon from an Atlantic MORB glass: concentration, distribution and isotopic composition. Earth Planet. Sci. Lett. 73, 255–268.
Javoy, M., Pineau, F., 1991. The volatiles record of a "popping" rock from the Mid-Atlantic Ridge at 14°N: chemical and isotopic composition of gas trapped in the vesicles. Earth Planet. Sci. Lett. 107, 598–611.
Javoy, M., Pineau, F., Allègre, C.J., 1982. Carbon geodynamic cycle. Nature 300, 171–173.
Jean-Baptiste, P., 1992. Helium-3 distribution in the deep world ocean. In: Rozanski, K. (Ed.), Isotopes of Noble Gases as Tracers in Environmental Studies. International Atomic Energy Agency, Vienna, pp. 219–240.
Johnson, K.T., Dick, H.J.B., Shimizu, N., 1990. Melting in the oceanic upper mantle: an ion microprobe study of diopsides in abyssal peridotites. J. Geophys. Res. 95, 2661–2678.
Kagoshima, T., Sano, Y., Takahata, N., Maruoka, T., Fischer, T.P., Hattori, K., 2015. Sulphur geodynamic cycle. Sci. Rep. 5 (8330).
Kellogg, L.H., Wasserburg, G.J., 1990. The role of plumes in mantle helium fluxes. Earth Planet. Sci. Lett. 99, 276–289.
Kendrick, M.A., Honda, M., Pettke, T., Scambelluri, M., Phillips, D., Giuliani, A., 2013. Subduction zone fluxes of halogens and noble gases in seafloor and forearc serpentinites. Earth Planet. Sci. Lett. 365, 86–96.
Kendrick, M.A., Scambelluri, M., Honda, M., Phillips, D., 2011. High abundances of noble gas and chlorine delivered to the mantle by serpentinite subduction. Nat. Geosci. 4, 807–812.
Klein, E.M., Langmuir, C.H., 1987. Global correlations of ocean ridge basalt chemistry with axial depth and crustal thickness. J. Geophys. Res. 92, 8089–8115.

Le Voyer, M., Kelley, K.A., Cottrell, E., Hauri, E.H., 2017. Heterogeneity in mantle carbon content from CO_2-undersaturated basalts. Nat. Commun. 8, 14062.
Lux, G., 1987. The behavior of noble gases in silicate liquids: solution, diffusion, bubbles and surface effects, with applications to natural samples. Geochim. Cosmochim. Acta 51, 1549–1560.
Marty, B., 1995. Nitrogen content of the mantle inferred from N_2–Ar correlation in oceanic basalts. Nature 377, 326–329.
Marty, B., 2012. The origins and concentrations of water, carbon, nitrogen and noble gases on Earth. Earth Planet. Sci. Lett. 313, 56–66.
Marty, B., Dauphas, N., 2003. The nitrogen record of crust–mantle interaction and mantle convection from Archean to Present. Earth Planet. Sci. Lett. 206, 397–410.
Marty, B., Jambon, A., 1987. $C/^3He$ in volatile fluxes from the solid Earth: implications for carbon geodynamics. Earth Planet. Sci. Lett. 83, 16–26.
Marty, B., Tolstikhin, I.N., 1998. CO_2 fluxes from mid-ocean ridges, arcs and plumes. Chem. Geol. 145, 233–248.
Marty, B., Zimmermann, L., 1999. Volatiles (He, C, N, Ar) in mid-ocean ridge basalts: assessment of shallow-level fractionation and characterization of source composition. Geochim. Cosmochim. Acta 63, 3619–3633.
Matsuda, J.I., Marty, B., 1995. The $^{40}Ar/^{36}Ar$ ratio of the undepleted mantle; a reevaluation. Geophys. Res. Lett. 22, 1937–1940.
Matthews, S., Shorttle, O., Rudge, J.F., Maclennan, J., 2017. Constraining mantle carbon: CO_2-trace element systematics in basalts and the roles of magma mixing and degassing. Earth Planet. Sci. Lett. 480, 1–14.
Michael, P.J., Graham, D.W., 2015. The behavior and concentration of CO_2 in the suboceanic mantle: inferences from undegassed ocean ridge and ocean island basalts. Lithos 236, 338–351.
Morbidelli, A., Chambers, J., Lunine, J.I., Petit, J.M., Robert, F., Valsecchi, G.B., Cyr, K.E., 2000. Source regions and timescales for the delivery of water to the Earth. Meteorit. Planet. Sci. 35, 1309–1320.
Moreira, M., Allègre, C.J., 2002. Rare gas systematics on Mid Atlantic ridge (37–40°N). Earth Planet. Sci. Lett. 198, 401–416.
Moreira, M., Sarda, P., 2000. Noble gas constraints on degassing processes. Earth Planet. Sci. Lett. 176, 375–386.
Moreira, M., Escartin, J., Gayer, E., Hamelin, C., Bezos, A., Guillon, F., Cannat, M., 2011. Rare gas systematics on Lucky Strike basalts (37°N, North Atlantic): evidence for efficient homogenization in a long-lived magma chamber system? Geophys. Res. Lett. 38, L08304.
Moreira, M., Kunz, J., Allègre, C., 1998. Rare gas systematics in popping rock: isotopic and elemental compositions in the upper mantle. Science 279, 1178–1181.
Moreira, M., Staudacher, T., Sarda, P., Schilling, J.G., Allègre, C.J., 1995. A primitive plume neon component in MORB: the Shona ridge-anomaly, South Atlantic (51–52°S). Earth Planet. Sci. Lett. 133, 367–377.
Moreira, M., Valbracht, P.J., Staudacher, T., Allègre, C.J., 1996. Rare gas systematics in Red Sea ridge basalts. Geophys. Res. Lett. 23, 2453–2456.
Mukhopadhyay, S., 2012. Early differentiation and volatile accretion recorded in deep-mantle neon and xenon. Nature 486, 101–104.
Mundl, A., Touboul, M., Jackson, M.G., Day, J.M.D., Kurz, M.D., Lekic, V., Helz, R., Walker, R.J., 2017. Tungsten-182 heterogeneity in modern ocean island basalts. Science 356, 66–69.
Niedermann, S., Bach, W., 1998. Anomalously nucleogenic neon in North Chile Ridge basalt glasses suggesting a previously degassed mantle source. Earth Planet. Sci. Lett. 160, 447–462.
Niedermann, S., Bach, W., Erzinger, J., 1997. Noble gas evidence for a lower mantle component in MORBs from the southern East Pacific Rise: decoupling of helium and neon isotope systematics. Geochim. Cosmochim. Acta 61, 2697–2715.
Nowak, M., Schreen, D., Spickenbom, K., 2004. Argon and CO_2 on the race track in silicate melts: a tool for the development of a CO_2 speciation and diffusion model. Geochim. Cosmochim. Acta 68, 5127–5138.
O'Nions, R.K., Oxburgh, E.R., 1983. Heat and helium in the Earth. Nature 306, 429–431.
Pan, V., Holloway, J.R., Hervig, R.L., 1991. The pressure and temperature dependence of carbon dioxide solubility in tholeiitic basalt melts. Geochim. Cosmochim. Acta 55, 1587–1595.
Paonita, A., Martelli, M., 2007. A new view of the He–Ar–CO_2 degassing at mid-ocean ridges: homogeneous composition of magmas from the upper mantle. Geochim. Cosmochim. Acta 71, 1747–1763.
Parai, R., Mukhopadhyay, S., 2015. The evolution of MORB and plume mantle volatile budgets: constraints from fission Xe isotopes in Southwest Indian Ridge basalts. Geochem. Geophys. Geosyst. 16, 719–735.
Parai, R., Mukhopadhyay, S., Standish, J.J., 2012. Heterogeneous upper mantle Ne, Ar and Xe isotopic compositions and a possible Dupal noble gas signature recorded in basalts from the Southwest Indian Ridge. Earth Planet. Sci. Lett. 359, 227–239.
Pető, M.K., 2014. Application of Noble Gas Isotopic Systems to Identify Mantle Heterogeneities. Ph.D. Thesis. Harvard University, Cambridge.
Pineau, F., Javoy, M., 1983. Carbon isotopes and concentrations in mid-oceanic ridge basalts. Earth Planet. Sci. Lett. 62, 239–257.
Pineau, F., Javoy, M., 1994. Strong degassing at ridge crests: the behaviour of dissolved carbon and water in basalt glasses at 14°N, Mid-Atlantic Ridge. Earth Planet. Sci. Lett. 123, 179–198.
Pineau, F., Javoy, M., Bottinga, Y., 1976. $^{13}C/^{12}C$ ratios of rocks and inclusions in popping rocks of the Mid-Atlantic Ridge and their bearing on the problem of isotopic composition of deep-seated carbon. Earth Planet. Sci. Lett. 29, 413–421.
Porcelli, D., Ballentine, C.J., 2002. Models for distribution of terrestrial noble gases and evolution of the atmosphere. Rev. Mineral. Geochem. 47, 411–480.
Porcelli, D., Wasserbug, G.J., 1995. Mass transfer of helium, neon, argon, and xenon through a steady-state upper mantle. Geochim. Cosmochim. Acta 59, 4921–4937.
Ragettli, R.A., Hebeda, E.H., Signer, P., Wieler, R., 1994. Uranium–xenon chronology: precise determination of λ_{sf*} $^{136}Y_{sf}$ for spontaneous fission of ^{238}U. Earth Planet. Sci. Lett. 128, 653–670.
Raquin, A., Moreira, M., 2009. Atmospheric $^{38}Ar/^{36}Ar$ in the mantle: implications for the nature of the terrestrial parent bodies. Earth Planet. Sci. Lett. 287, 551–558.
Raquin, A., Moreira, M.A., Guillon, F., 2008. He, Ne and Ar systematics in single vesicles: mantle isotopic ratios and origin of the air component in basaltic glasses. Earth Planet. Sci. Lett. 274, 142–150.
Rosenthal, A., Hauri, E.H., Hirschmann, M.M., 2015. Experimental determination of C, F, and H partitioning between mantle minerals and carbonated basalt, CO_2/Ba and CO_2/Nb systematics of partial melting, and the CO_2 contents of basaltic source regions. Earth Planet. Sci. Lett. 412, 77–87.
Saal, A.E., Hauri, E.H., Langmuir, C.H., Perfit, M.R., 2002. Vapour undersaturation in primitive mid-ocean-ridge basalt and the volatile content of Earth's upper mantle. Nature 419, 451–455.
Sarda, P., Graham, D., 1990. Mid-ocean ridge popping rocks: implications for degassing at ridge crests. Earth Planet. Sci. Lett. 97, 268–289.
Sarda, P., Moreira, M., 2002. Vesiculation and vesicle loss in mid-ocean ridge basalt glasses: He, Ne, Ar elemental fractionation and pressure influence. Geochim. Cosmochim. Acta 66, 1449–1458.
Sarda, P., Moreira, M., Staudacher, T., Schilling, J.G., Allègre, C.J., 2000. Rare gas systematics on the southernmost Mid-Atlantic Ridge: constraints on the lower mantle and the Dupal source. J. Geophys. Res., Solid Earth 105, 5973–5996.
Shaw, A.M., Behn, M.D., Humphris, S.E., Sohn, R.A., Gregg, P.M., 2010. Deep pooling of low degree melts and volatile fluxes at the 85°E segment of the Gakkel Ridge: evidence from olivine-hosted melt inclusions and glasses. Earth Planet. Sci. Lett. 289, 311–322.
Shimizu, K., Saal, A.E., Myers, C.E., Nagle, A.N., Hauri, E.H., Forsyth, D.W., Kamenetsky, V.S., Niu, Y., 2016. Two-component mantle melting–mixing model for the generation of mid-ocean ridge basalts: implications for the volatile content of the Pacific upper mantle. Geochim. Cosmochim. Acta 176, 44–80.
Sleep, N.H., Zahnle, K., 2001. Carbon dioxide cycling and implications for climate on ancient Earth. J. Geophys. Res., Planets 106, 1373–1399.
Šrámek, O., Stevens, L., McDonough, W.F., Mukhopadhyay, S., Peterson, R.J., 2017. Subterranean production of neutrons, ^{39}Ar and ^{21}Ne: rates and uncertainties. Geochim. Cosmochim. Acta 196, 370–387.
Stolper, E., Holloway, J.R., 1988. Experimental determination of the solubility of carbon dioxide in molten basalt at low pressure. Earth Planet. Sci. Lett. 87, 397–408.
Stroncik, N.A., Niedermann, S., 2016. Atmospheric contamination of the primary Ne and Ar signal in mid-ocean ridge basalts and its implications for ocean crust formation. Geochim. Cosmochim. Acta 172, 306–321.
Stroncik, N.A., Niedermann, S., Haase, K.M., 2007. Neon and helium isotopes as tracers of mantle reservoirs and mantle dynamics. Earth Planet. Sci. Lett. 258, 334–344.
Tackley, 2015. Mantle geochemical dynamics. In: Schubert, G. (Ed.), Treatise on Geophysics, 2nd ed. Elsevier, Amsterdam, pp. 521–585.
Trieloff, M., Kunz, J., 2005. Isotope systematics of noble gases in the Earth's mantle: possible sources of primordial isotopes and implications for mantle structure. Phys. Earth Planet. Inter. 148, 13–38.
Tucker, J.M., Mukhopadhyay, S., 2014. Evidence for multiple magma ocean outgassing and atmospheric loss episodes from mantle noble gases. Earth Planet. Sci. Lett. 393, 254–265.
Tucker, J.M., Mukhopadhyay, S., Schilling, J.G., 2012. The heavy noble gas composition of the depleted MORB mantle (DMM) and its implications for the preservation of heterogeneities in the mantle. Earth Planet. Sci. Lett. 355, 244–254.
Van Keken, P.E., Ballentine, C.J., Porcelli, D., 2001. A dynamical investigation of the heat and helium imbalance. Earth Planet. Sci. Lett. 188, 421–434.
Walker, J.C., Hayes, P.B., Kasting, J.F., 1981. A negative feedback mechanism for the long-term stabilization of Earth's surface temperature. J. Geophys. Res. 86, 9776–9782.
Wänke, H., 1981. Constitution of terrestrial planets. Philos. Trans. R. Soc. Lond. A 303, 287–302.
Wanless, V.D., Shaw, A.M., 2012. Lower crustal crystallization and melt evolution at mid-ocean ridges. Nat. Geosci. 5, 651–655.
Wanless, V.D., Behn, M.D., Shaw, A.M., Plank, T., 2014. Variations in melting dynamics and mantle compositions along the Eastern Volcanic Zone of the Gakkel Ridge: insights from olivine-hosted melt inclusions. Contrib. Mineral. Petrol. 167, 1–22.

Wanless, V.D., Shaw, A.M., Behn, M.D., Soule, S.A., Escartín, J., Hamelin, C., 2015. Magmatic plumbing at Lucky Strike volcano based on olivine-hosted melt inclusion compositions. Geochem. Geophys. Geosyst. 16, 126–147.

Watson, E.B., Sneeringer, M.A., Ross, A., 1982. Diffusion of dissolved carbonate in magmas: experimental results and applications. Earth Planet. Sci. Lett. 61, 346–358.

Weston, B., Burgess, R., Ballentine, C.J., 2015. Disequilibrium degassing model determination of the ^{3}He concentration and ^{3}He/^{22}Ne of the MORB and OIB mantle sources. Earth Planet. Sci. Lett. 410, 128–139.

Yamamoto, J., Burnard, P.G., 2005. Solubility controlled noble gas fractionation during magmatic degassing: implications for noble gas compositions of primary melts of OIB and MORB. Geochim. Cosmochim. Acta 69, 727–734.

Yatsevich, I., Honda, M., 1997. Production of nucleogenic neon in the Earth from natural radioactive decay. J. Geophys. Res., Solid Earth 102, 10291–10298.

Zhang, Y., Stolper, E.M., 1991. Water diffusion in a basaltic melt. Nature 351, 306–309.